New Anomalies in Cosmic Microwave Background Anisotropy: Violation of the Isotropic Gaussian Hypothesis in Low-l Modes

Shi Chun, Su and M.-C., Chu[y]

Department of Physics and Institute of Theoretical Physics,

The Chinese University of Hong Kong, Shatin, Hong Kong

(Dated: February 20, 2024)

Abstract

In the standard framework of cosmology, primordial density fluctuations are assumed to have an isotropic Gaussian distribution. We search for deviations from this assumption in the WMAP data for the low l modes of Cosmic Microwave Background Anisotropies (CMBA), by studying the directions of the z-axis that maximize the $l = m$ modes and the resulting amplitudes of these modes. We find a general alignment of the directions for $l = 2$ to 10 modes to within 1/4 of the northern hemisphere. This alignment can be regarded as a generalization of the recently discovered alignment of the $l = 2$ and 3 modes – the so-called 'Axis of Evil'. Furthermore, we find abnormally high (low) powers in the $l = m = 6, 12 - 17$ ($l = m = 5$) modes; the probabilities for having the anomalous amplitudes of the $l = m = 5, 6, 17$ modes are about 0.1%, 1% and 1% respectively according to the Gaussian conjecture. The alignment and anomalous amplitudes for these low l modes are very robust against foreground contamination or different cleaning strategies, suggesting a cosmological origin and possibly supporting a non-standard inflation.

PACS numbers: 98.80.Es, 95.75.Pq, 98.70.Vc

Electronic address: scsu@phy.cuhk.edu.hk

[y]Electronic address: mcchu@phy.cuhk.edu.hk

Modern theories of cosmology are based on three postulates: homogeneity and isotropy of the Universe, and primordial fluctuations of density. These three postulates have been verified to a large extent by the observation of the Cosmic Microwave Background Anisotropies (CMBA) and the large scale structures of the Universe. One usually assumes that the fluctuations are statistically isotropic and Gaussian. Therefore, when one expands the temperature anisotropy $T(\theta,\phi) = T(\theta,\phi) - T_0$ ($T_0 = 2.73K$ is the mean blackbody temperature today) of the CMBA observed today into spherical harmonics:

$$T(\theta,\phi) = \sum_{l=1}^{\infty} \sum_{m=-l}^{l} a_{lm} Y_{lm}(\theta,\phi), \tag{1}$$

the a_{lm}'s are expected to follow a gaussian distribution among different samples of the Last Scattering Surface (LSS) as seen from different locations of the Universe. Unfortunately, we can observe a sample of the LSS at a particular time in a particular position only. There is inevitably a statistical uncertainty (cosmic variance), no matter how accurate our observation is.

Recently, some anomalies in the WMAP data for low l's, which are found to be inconsistent with the isotropic gaussian hypothesis (IGH) of the primordial fluctuations, are widely studied (e.g., [1, 2, 3, 4, 5, 6, 7]). The most famous anomalies are the low quadrupole amplitude C_2, where $(2l+1)C_l = \sum_{m=-l}^{l} |a_{lm}|^2$, and the alignment of multipoles for $l = 2$ and 3, which is known as the 'Axis of Evil' (AOE). Although some may argue that we may just be observing a 'strange' universe by accident due to the cosmic variance, many other suggestions have been offered to explain the anomalies (e.g., [8, 9, 10, 11, 12, 13, 14]). Some claim that the foreground contaminations (e.g., [11, 12]), especially those from the galactic plane or the Virgo supercluster (towards where the alignment of $l = 2$ and 3 multipoles directs), may give rise to the anomalies. The foreground-cleaning strategies commonly used cannot provide CMBA maps that are free of foreground contamination residues. More interestingly, some propose that the anomalies are true anisotropic signals from the early Universe and suggest possible mechanisms of producing them (e.g., [13, 14]). It is of obvious importance and interest to distinguish among these three possibilities.

In this paper, we discuss several new anomalies which will make it more difficult to attribute the anomalies to coincidence. We also analyze how the galactic plane and other foreground contaminations affect the anomalies and show that they most likely do not give rise to the anomalies.

We analyze

$$r_{lm} \quad \max_{\hat{n}} \begin{cases} \frac{|a_{l0}|^2}{(2l+1)C_l}; & m = 0 \\ \frac{2|a_{lm}|^2}{(2l+1)C_l}; & m \neq 0. \end{cases} \tag{2}$$

Here, r_{lm} measures the maximum contribution of the multipole $(l;m)$ to the temperature power spectrum among all possible directions $\hat{n}$ of the z-axis (= 0). We denote the direction $\hat{n}$ where r_{lm} is found as $\hat{n}_{max}$. Equation (2) provides not only a measurement of the multipoles' alignment, but also an indication of how dominant a multipole is over other m modes of the same l. In [6], $r_l = \max_m r_{lm}$ is studied instead of r_{lm}. However, the distribution of values of r_{lm}'s can be different for different m's of the same l in general, leading to different expectation values of r_{lm}. Therefore, $r_l = \max_m r_{lm}$ is biased to some particular multipoles m (m l=2) which have larger expectation values of r_{lm}. We therefore study r_{lm} separately.

We analyze the 3-year full-sky WMAP Internal Linear Combination (WILC3YR) map released by the WMAP team [15]. We also generate 100,000 Monte Carlo simulations with the IGH so as to study the statistical properties of r_{lm}'s and $\hat{n}_{max}$'s. These statistics are then used to determine if any of those r_{lm}'s and $\hat{n}_{max}$'s from the observed CMBA data are anomalous under the IGH.

In the lower right graph of the Fig. 1, we locate the directions $\hat{n}_{max}$ for l = m = 2 to 10, indicated by the corresponding numbers on a Mollweide projection of the sky for the WILC3YR map. The Galactic coordinate system is used and rotated by 180 around the z-axis for better view. The directions $\hat{n}_{max}$ are two-folded, i.e. a direction $\hat{n}_{max}$ of a multipole $(l;m)$ in the northern hemisphere must have a corresponding direction $-\hat{n}_{max}$ in the southern hemisphere giving the same value of r_{lm}. Here, we show only the $\hat{n}_{max}$'s of the multipoles in the northern hemisphere of the map. We find from the sky map that the directions $\hat{n}_{max}$ for l= m = 2 to 10 concentrate within 1/5 of the solid angle of the northern hemisphere. Furthermore, similar to the well-known alignment of the l= m = 2 and l= m = 3 multipoles, there is an equally strong alignment of the l= m = 5 and l= m = 6 multipoles. The probability to have such a new AOE under the IGH is only 1%.

In Fig. 2, the values of r_{ll}'s from the WILC3YR map are shown against l by the 'star' symbols while the lines indicate the median and 99% confidence levels (solid and dash lines) of the 100,000 Monte Carlo data under the IGH. From Fig. 2, we see that the values of r_{ll}'s from the WILC3YR map show a general decreasing trend as l increases. This trend

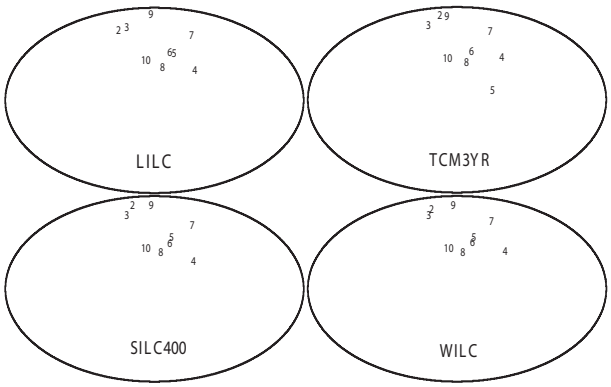

FIG. 1: The Mollweide projection of the full sky showing the directions $\hat{n}_{max}$ of $l = m = 2$ to 10 multipoles (indicated by the corresponding numbers) in the four different foreground-cleaned CMBA maps: LILC, SILC400, TCM3YR and WILC3YR map. The sky maps are rotated by 180 around the z-axis for better view. The directions $\hat{n}_{max}$ are two-folded with respect to the origin. Only those $\hat{n}_{max}$'s in the northern hemisphere are shown.

is consistent with the averaged values of the simulated r_{ll}'s under the IGH. Also, most r_{ll}'s obtained from the WILC3YR map are consistent with these expected values within 90% confidence level with a few exceptions. First, we find that r_{55} obtained from the WILC3YR map is much smaller than the IGH's median of r_{55}. The probability to have such a small r_{55} with the IGH is about 0.1%. Second, another interesting but less significant anomaly is the unusually large value of r_{66}. This anomaly can be reproduced by the IGH with about 1% chance. Third, from $l = 12$ to 16, the values of r_{ll} from observational data are all slightly larger than the IGH's median rather than fluctuating around the latter. Finally, r_{11} for $l = 17$ is abnormally large, with a value that has less than 1% probability under the IGH, and it also aligns with the directions $\hat{n}_{max}$ for $l = m = 5$ and 6 to within 5°.

We study how robust these anomalies are in several ways:

Different cleaning methods

We apply the same analysis to three other foreground-cleaned WMAP maps: LILC [16], SILC400 [17] and TCM3YR [18]. Their directions $\hat{n}_{max}$ of $l = m$ multipoles are shown in Fig. 1 together with those of the WILC3YR map. We can see that almost all the $\hat{n}_{max}$ are consistent for the four CMBA maps. The only exception is the $l = m = 5$ multipole from

TCM3YR which shows a weaker alignment with the $l = m = 6$ multipole. Nevertheless, the general alignment for $l = m = 2$ to 10 multipoles is still strong. Even for the worst case (TCM3YR), these directions $\hat{n}_{max}$ concentrate within 1/4 solid angle of the north hemisphere. The fact that a strong alignment of $l = m = 5$ and 6 multipoles persists in the other three maps suggests that it is a true anomaly. We also perform the same analysis on the WILC map with the 5-year data [19] (not shown). The directions $\hat{n}_{max}$ for all l's from 2 to 10 are consistent with those of the 3-year data except that for $l = 8$ points to a very different direction.

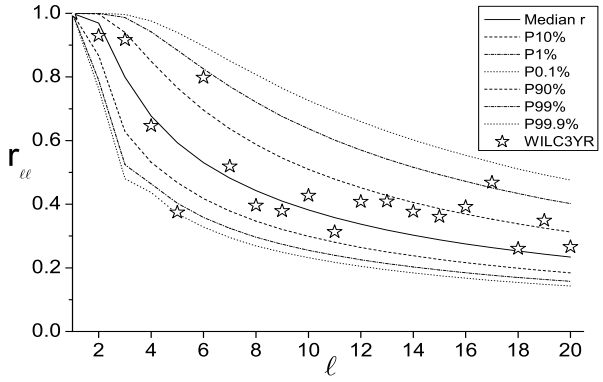

FIG. 2: The values of r_{ll} calculated from the WILC 3YR map against l are shown as stars, compared to statistical values under the IGH (lines). r_{55} (r_{66}) is significantly smaller (larger) than the corresponding medians under the IGH, shown by the solid line. r_{ll} for $l = 17$ is abnormally large too.

In Fig. 3, we show the values of r_{ll}'s from all four foreground-cleaned CMBA maps. We can see that the dependence of the r_{ll}'s on different cleaning schemes are small for most l's from 2 to 20. This consistency suggests that all anomalies mentioned above are robust features. In particular, the negligible dispersion of r_{55} keeps the probability of having such a small value of r_{55} as 0.1%. Although the value of r_{66} from the TCM3YR map is significantly less than those of the other three maps, it is still well above the 90% probability region under the IGH. Similarly, the anomaly of r_{ll} for $l = 17$ is still present for all the four foreground-cleaned maps. Also, the surge of r_{ll} from $l = 12$ to 16 over their IGH's median persists. We remark that the dispersion of r_{44} is exceptionally large but it is not related to any anomalies.

Effects of the foreground contaminations

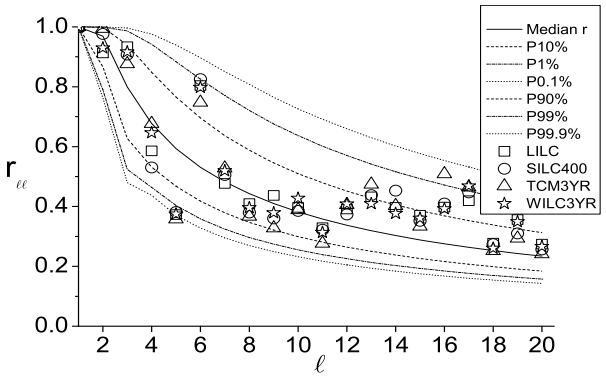

FIG. 3: Same as Fig. 2, but with data from all the four foreground-cleaned CMB maps.

In order to examine the effects of the foreground contaminations on the anomalies, we introduce a simple but aggressive method: a region of the CMBA map is replaced by a weighted average of the CMBA T and a simulated T_{IGH} under the IGH, i.e. $T' = \alpha T + (1-\alpha) T_{IGH}$, where T is the observed temperature anisotropy and α ranges from 0 to 1. It is possible that the foreground contaminations as a deterministic effect changes the statistical properties of the CMBA signals under the IGH, e.g. shifting the mean values of r_{lm} and concentrating the directions $\hat{n}_{max}$. Conversely, the persistence of the anomalies after the replacement assures us that these foreground contaminations cannot independently produce the anomalies. The method is aggressive because it erases partially the real signals from LSS (which may violate the IGH itself) as well as the contaminations. If the anomalies are eliminated after the substitution, it is difficult, if not impossible, to distinguish between the contributions due to loss of real signals and contaminations. Therefore, the analysis is good at excluding contaminations as a candidate of explaining the anomalies but not at supporting it. The advantage of using this method is that it is valid even for dealing with unknown contamination residues. We apply the method to study the effects of the foreground contaminations on the galactic plane (plus point sources) and at the Virgo supercluster as potential sources to produce the anomalies.

For the galactic plane, we use the widely used standard intensity mask – kp2, which covers 15.3% of the full sky including the galactic plane and point sources, as the region of the replacement, and α is set to be 0.5. The averaged values of r_{ll}'s of the modified maps over 1000 simulations are plotted against l in Fig. 4. We can see that all anomalies of r_{ll}'s

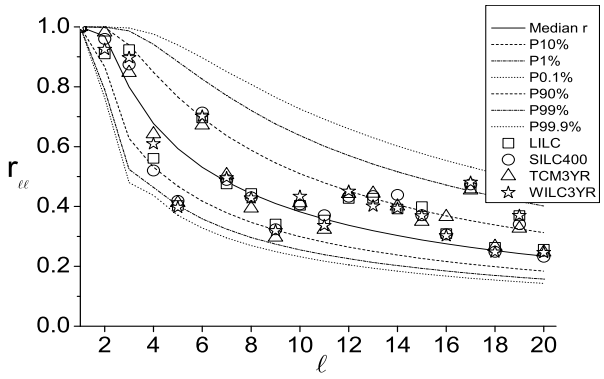

FIG. 4: Same as Fig. 3, but the values of r_{lm}'s are averages of r_{lm}'s obtained from the mask-replaced maps through 1000 simulations under the IGH with $= 0.5$.

mentioned above are still significant. The depressed (boosted) value of r_{55} (r_{66}) remains at about 1% (10%) probability under the IGH. The surge of values of r_{ll}'s from $l = 12$ to 16 still exists obviously, and the value of $r_{17,17}$ is still abnormal at about 99% confidence level. The directions $\hat{n}_{max}$ for $l = 2, 3, 4, 6, 7$ and 10 under replacements stay near their original directions. Although those for $l = 5, 8$ and 9 may point away to other possible directions, they gather in different patches respectively instead of spreading all over the sky. Among these patches, only one for $l = 5$ and one for $l = 8$ direct outsides the original region of the concentration or the generalized AOE.

In order to test if the anomalies are caused by the foreground contamination at the Virgo supercluster, we replace 50% of signals from the Virgo supercluster by simulated data under the IGH. The results for r_{ll}'s are shown in Fig. 5. r_{55}, r_{66}, and $r_{17,17}$ are still anomalous at over 99%, 90% and 90% level respectively and the surge for $l = m = 12$ to 16 remains. Furthermore, such a replacement does not affect the general alignment of the low lm modes, with only the $\hat{n}_{max}$ of $l = m = 8$ pointing away from the generalized AOE for the TCM 3YR map. We will give more details on how the $\hat{n}_{max}$'s change under foreground contaminations in a coming paper.

The general alignment of the directions $\hat{n}_{max}$'s for $l = 2$ to 10 within $1/4$ of the northern hemisphere is very robust and is unlikely to be eliminated by foreground contaminations or cleaning strategies. Furthermore, the anomalies of r_{55}, r_{66}, $r_{17,17}$ and the surge of r_{ll}'s for

$l = 12$ to 16 together are highly inconsistent with the IGH and robust against foreground cleanings. In fact, the values of r_{55}, r_{66} and $r_{17;17}$ are anomalous under the IGH at about 10^{3}, 10^{2} and 10^{2} levels respectively, which is extremely 'strange' by coincidence. Our results therefore favor true cosmological origins of the anomalies and possibly support a non-standard in ation.

Our analysis made use of HEALPIX [20, 21]. This work is supported by grants from the Research Grant Council of the Hong Kong Special Administrative Region, China (Project Nos. 400707 and 400803).

---

[1] A. de Oliveira-Costa et al:, Phys. Rev. D 69, 063516 (2004).

[2] F. K. Hansen et al:, Astrophys. J. 607, L67 (2004).

[3] P. Vielva et al:, Astrophys. J. 609, 22 (2004).

[4] H. K. Eriksen et al:, Astrophys. J. 612, 633 (2004).

[5] D. J. Schwarz et al:, Phys. Rev. Lett. 93, 221301 (2004).

[6] K. Land et al:, Phys. Rev. Lett. 95, 071301 (2005).

[7] C. J. Copi et al:, Phys. Rev. D 70, 043515 (2004).

[8] T. R. Ja e et al:, Astrophys. J. 629L, 1J (2005).

[9] L. Campanelli et al:, Phys. Rev. Lett. 97, 131302 (2006).

[10] N. J. Cornish et al:, Phys. Rev. Lett. 92, 20 (2004).

[11] K. T. Inoue et al:, Astrophys. J. 648, 23I (2006).

[12] C. Vale et al:, preprint, [astro-ph/0509039].

[13] Y. S. Piao et al:, Phys. Rev. D 71, 087301 (2005).

[14] B. Feng et al:, Phys. Lett. B 570, 145 (2003).

[15] The 3-year WMAP ILC map is available at
http://lambda.gsfc.nasa.gov/product/map/dr2/m_products.cfm .

[16] The LILC map is available at
http://www.astro.uio.no/ hke/cmbdata/WMAP_ILC_lagrange. ts.

[17] The SILC400 map is available at
http://newton.kias.re.kr/ parkc/CMB/SILC400.html.

[18] The TCM 3YR map is available at

http://space.mit.edu/home/tegmark/wmap.html.

[19] The 5-year WMAP ILC map is available at

http://lambda.gsfc.nasa.gov/product/map/current/m_products.cfm.

[20] K.M. Gorski et al., Astrophys. J. 622, 759 (2005).

[21] Healpix is available at

http://healpix.jpl.nasa.gov

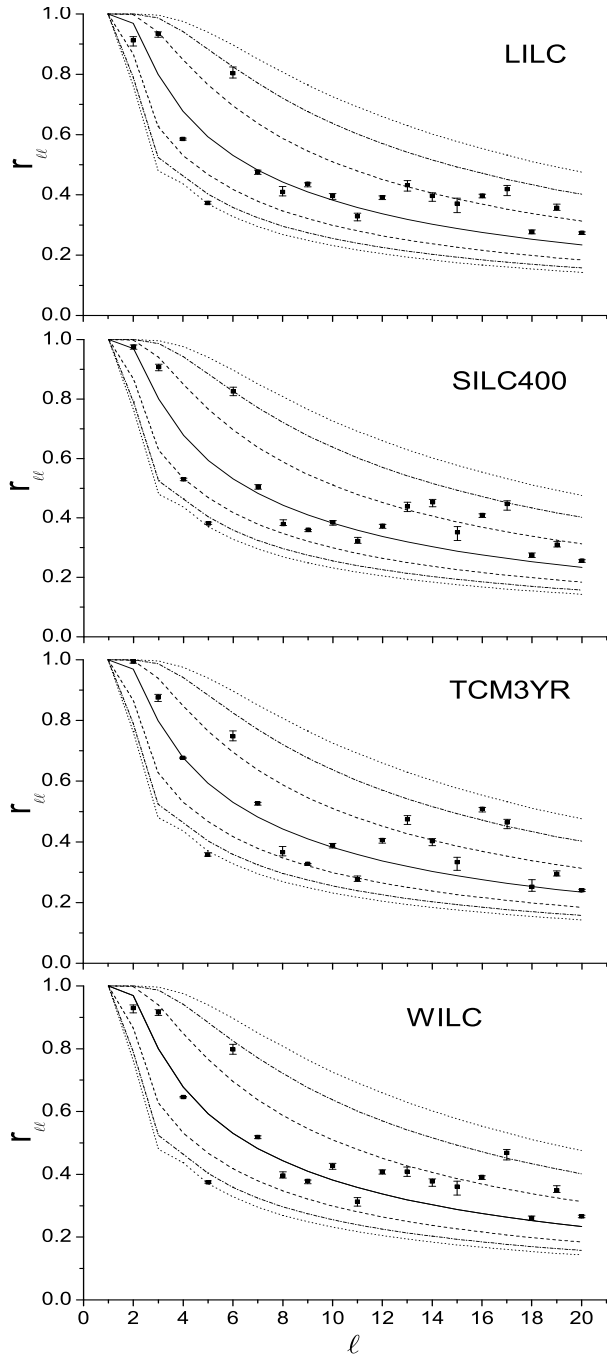

FIG. 5: Same as Fig.2, but for each l, the square indicates the original value of r_{ll}. The ends of the error bar indicate the upper and lower standard deviations of the simulated values of r_{ll} (over 1,000 simulations) produced by replacing the patch of the Virgo Supercluster by the IGH signals.